HHS Public Access

Author manuscript

Cancer Res. Author manuscript; available in PMC 2019 July 01.

Published in final edited form as:

Cancer Res. 2018 July 01; 78(13): 3445–3457. doi:10.1158/0008-5472.CAN-17-2928.

GFPT2-expressing cancer-associated fibroblasts mediate metabolic reprogramming in human lung adenocarcinoma

Weiruo Zhang[1], **Gina Bouchard**[1], **Alice Yu**[1], **Majid Shafiq**[1], **Mehran Jamali**[1], **Joseph Shrager**[2], **Kelsey Ayers**[1], **Shaimaa Bakr**[3], **Andrew J. Gentles**[4], **Maximilian Diehn**[5], **Andrew Quon**[6], **Robert West**[7], **Viswam S. Nair**[8], **Matt van de Rijn**[7], **Sandy Napel**[1], and **Sylvia K. Plevritis**[1,4,*]

[1]Department of Radiology, Stanford University School of Medicine, 291 Campus Drive, Stanford, CA 94305, USA

[2]Division of Thoracic Surgery, Department of Cardiothoracic Surgery, Stanford University School of Medicine, 291 Campus Drive, Stanford, CA 94305, USA and Veterans Affairs Palo Alto Health Care System, 3801 Miranda Avenue, Palo Alto, CA 94304, USA

[3]Department of Electrical Engineering, Stanford University, 650 Serra Mall, Stanford, CA 94305, USA

[4]Department of Biomedical Data Science, Stanford University School of Medicine, 291 Campus Drive, Stanford, CA 94305, USA

[5]Department of Radiation Oncology, Stanford University School of Medicine, 875 Blake Wilbur Drive, Stanford, CA 94305, USA

[6]David Geffen School of Medicine, UCLA, 200 Med Plaza, Los Angeles, CA 90095, USA

[7]Department of Pathology, Stanford University School of Medicine, 300 Pasteur Drive, Stanford, CA 94305, USA

[8]Canary Center at Stanford for Cancer Early Detection, 3155 Porter Drive, Palo Alto, CA 94305 USA

Abstract

Metabolic reprogramming of the tumor microenvironment is recognized as a cancer hallmark. To identify new molecular processes associated with tumor metabolism, we analyzed the transcriptome of bulk and flow-sorted human primary non-small cell lung cancer (NSCLC) together with ^{18}FDG-positron emission tomography scans, which provide a clinical measure of glucose uptake. Tumors with higher glucose uptake were functionally enriched for molecular processes associated with invasion in adenocarcinoma (AD) and cell growth in squamous cell carcinoma (SCC). Next, we identified genes correlated to glucose uptake that were predominately overexpressed in a single cell-type comprising the tumor microenvironment. For SCC, most of these genes were expressed by malignant cells, whereas in AD they were predominately expressed

Corresponding author: Sylvia K. Plevritis, James H. Clark Center, 318 Campus Drive, Room S255, Stanford, CA 94305, USA. Phone: 650-498-5261; Fax: 650-724-9113; sylvia.plevritis@stanford.edu.

Competing interests: The authors declare no potential conflicts of interest.

by stromal cells, particularly cancer-associated fibroblasts (CAFs). Among these AD genes correlated to glucose uptake, we focused on Glutamine-Fructose-6-Phosphate Transaminase 2 (GFPT2), which codes for the Glutamine-Fructose-6-Phosphate Aminotransferase 2 (GFAT2), a rate-limiting enzyme of the hexosamine biosynthesis pathway (HBP), which is responsible for glycosylation. GFPT2 was predictive of glucose uptake independent of GLUT1, the primary glucose transporter, and was prognostically significant at both gene and protein level. We confirmed that normal fibroblasts transformed to CAF-like cells, following TGF-β treatment, upregulated HBP genes, including GFPT2, with less change in genes driving glycolysis, pentose phosphate pathway and TCA cycle. Our work provides new evidence of histology-specific tumor-stromal properties associated with glucose uptake in NSCLC and identifies GFPT2 as a critical regulator of tumor metabolic reprogramming in AD.

Introduction

Cancer is known to have altered metabolism through the glycolysis pathway to meet demands for tumor growth. This phenomenon, termed the “Warburg effect” [1] is widely accepted, yet alterations in tumor metabolism are not restricted to enabling tumor growth but also promoting tumor invasion and metastatic progression [2]. This broader perspective has established metabolic reprogramming as a “cancer hallmark” [2,3]. Recent studies are revealing substantial metabolic heterogeneity in tumors [4,5]. Moreover, increasing consideration is being given to metabolic reprogramming of stromal cells comprising the tumor microenvironment (TME) [6]. For example, cancer-associated fibroblasts (CAFs), a major component in tumor stroma, have been reported to have increased glycolysis and produce high-energy nutrients that facilitate biogenesis in malignant cells, a process referred to as the “reverse Warburg effect” [7]. In support of these findings, studies have reported that malignant cells and CAFs express different monocarboxylate transporters (MCTs) for the consumption and production of lactate [8]. In this study, we provide new evidence of prognostically significant changes in the tumor stroma related to metabolic reprogramming of human non-small cell lung carcinoma.

Lung cancer remains the number one cause of cancer mortality in the United States, where non-small cell lung cancer (NSCLC) constitutes around 85% of lung cancer cases [9]. NSCLC has two major histology subtypes, namely adenocarcinoma (AD) and squamous cell carcinoma (SCC). AD and SCC are known to differ in their cell of origin and distribution across the lung [10–12]. They also differ in terms of glucose uptake as measured by ^{18}Fluoro-2-deoxy-D-glucose positron emission tomography (^{18}FDG-PET) scans: SCC has been associated with higher levels of uptake than AD. Consistent with these findings, SCC has higher expression of the glycolysis markers GLUT1 (SLC2A1), CA9 and MCT1 (SLC16A1) [13]. Even though higher glucose uptake in general is associated with more aggressive disease, SCC has been associated with better survival outcomes than AD among symptomatically detected patients [13]. However, it remains unclear how histology-related differences in glucose metabolism are related to cancer progression.

We assembled a study cohort of NSCLC patients for whom resected tumor specimens were acquired for transcriptomic analysis. To relate gene expression to metabolism, we also

acquired a preoperative ^{18}FDG-PET uptake feature, namely the maximum standardized uptake value (SUV_{max}), which is a common clinical measure of glucose uptake in human tumors in-vivo. We found that genes associated with glucose uptake in AD vs. SCC cases were functionally enriched for invasion vs. growth, respectively. From the transcriptome of flow-sorted NSCLC, we identified genes correlated with glucose uptake that were predominately expressed in a single cell-type comprising the tumor microenvironment. For SCC, the majority of these genes were expressed in malignant cells, whereas they were expressed in stromal cells of AD. In AD, we focused on Glutamine-Fructose-6-Phosphate Transaminase 2 (GFPT2) because we found it to be a prognostically significant glucose-related metabolic gene that was predominately expressed in the tumor stroma. GFPT2 is a rate-limiting gene of the hexosamine biosynthesis pathway (HBP), known to glycosylate proteins yet underreported in its relevance to cancer. Our analysis identifies a significant role for GFPT2 in AD CAFs, in association with extracellular matrix remodeling mediated through the hexosamine biosynthesis pathway. Overall, our findings provide new evidence of the histology-specific tumor-stromal functional properties associated with metabolic reprogramming in NSCLC and potential new therapeutic avenues.

Materials and Methods

Overview

We performed an integrative analysis of primary NSCLC with data obtained on medical imaging (^{18}FDG-PET), tissue microarray, transcriptomics, protein expression and survival outcomes across multiple cohorts and studies, as detailed below. Briefly, our primary cohort is our radiogenomics (RG) cohort (n=130) on which we relate SUV_{max} and bulk tumor gene expression. In addition, we assembled a companion tumor microenvironment (TME) NSCLC cohort (n=40) from which we used fluorescence-activated cell sorting (FACS) to sort major cell-types of the tumor microenvironment in order to determine which cell-type, if any, predominately expressed a specific gene of interest. In addition, we constructed a separate validation cohort, tissue microarray analysis (TMA) cohort (n=211), to validate the specific findings associated with glucose uptake and survival outcomes on the protein level. A workflow is provided in Supplement 1 Figure S1. Throughout our analysis, we focus on various gene sets, including: *genes correlated with glucose uptake* are defined as genes significantly correlated to SUV_{max} in our RG cohort; *cell-type-specific genes* are defined as genes predominately expressed in one cell-type comprising the tumor microenvironment, derived from our TME cohort; *prognostically significant genes* as determined by PRECOG database [14]; and *metabolic genes,* which were collated from metabolic-related pathways in Kyoto encyclopedia of genes and genomes (KEGG) [15] and HumanCyc [16]. For the metabolic genes, we focused only on genes associated with glucose uptake through the glucose transporter gene SLC2A1 (GLUT1) which shunt glucose into one of the three major pathways [17]: (i) the glycolysis pathway for energy production, (ii) the pentose phosphate pathway (PPP) for biomass production and (iii) the hexosamine biosynthesis pathway (HBP) for protein glycosylation.

Radiogenomics (RG) Cohort

Cohort Characteristics—With Institutional Review Board (IRB) approval in accordance with US Common Rule, we studied 130 patients with NSCLC who underwent curative surgical resection at Stanford University Hospital or Palo Alto VA Medical Center between year 2008 and 2015 and had a pre-operative PET/CT imaging. We refer to this cohort as our Radiogenomics (RG) cohort. Patient demographics of the study cohort were summarized in Table 1. Ninety-six AD and thirty-one SCC patients were included in the analysis (three cases were excluded due to undefined histology). Tissue samples ranged from 30mg–100mg and were flash-frozen. Transcriptomic data were obtained through RNA sequencing with data alignment and expression estimation performed via Centrillion Biosciences, Inc (Supplement 2). Preoperative PET/CT scans for tumor FDG uptake were paired to the tumor tissue specimens from which the RNA-seq data was generated. SUV_{max} was obtained by re-reading all 130 cases on MimVista software, guided by surgically reported information on excised lobe and slice to ensure the RNA-seq data and the annotated lesion were matched. Note that a preliminary analysis relating the transcriptome and the ^{18}FDG-PET features on the first 26 of 130 patients comprising our current RG cohort was reported by ourselves and others [18,19]. The current RG cohort RNA-seq data and imaging data are available at http://wiki.cancerimagingarchive.net/display/Public/NSCLC+Radiogenomics. A list of de-identified IDs of the patients used in the RG cohort is included in Supplement 3.

RNA-seq gene expression preprocessing and analysis—Genes detected in fewer than 50% samples were removed. The estimated gene expression profile using FPKM (Fragments Per Kilobase of transcript per Million mapped reads) was log-transformed and genes with variances in the lower 50% quartile were filtered out. RNA-seq profiling and data processing were performed in three batches through year 2014 to 2015. We observed significant batch effect between samples processed in 2014 and 2015 using principal component analysis (PCA) (Supplement 4 Figure S2) and applied COMBAT to adjust the batch effect [20]. Differentially expressed genes (DEG) between AD and SCC samples were identified using R package “multtest” based on permutation multiple testing [21]. A false discovery rate (FDR) of 5% was used to assess statistical significance.

Association of glucose uptake and gene expression—Correlation between glucose uptake, measured in terms of SUV_{max}, and individual gene expression was assessed by Spearman rank test on AD and SCC samples separately. To reduce false-positive correlations, we used Significance Analysis of Microarray (SAM) [22] to calculate a false discovery rate for each gene based on permutation testing using gene expression as features and SUV_{max} as a continuous outcome variable. For AD, significant correlations were defined with FDR lower than 10%. For SCC, due to the relatively smaller sample size, we increased the FDR threshold for significance to 20%. Genes correlated to glucose uptake were clustered using R package Weighted Correlation Network Analysis (WGCNA) [23] for AD and SCC separately. To identify the relevant biological functions of the gene clusters, we investigated the enriched gene ontology categories using MsigDB [24] and ToppFun [25]. We focused on cancer-related hallmark gene sets, biological processes and cellular components with FDR less than 5%.

Tumor Microenvironment (TME) Cohort

With Institutional Review Board (IRB) approval in accordance with US Common Rule, we studied 40 patients with NSCLC who underwent curative surgical resection at Stanford University Hospital or Palo Alto VA Medical Center between year 2008 and 2015. Hereon, we refer to this cohort as our Tumor Microenvironment (TME) cohort; this cohort enabled us to identify the cell-type specific contributions to metabolic reprogramming underlying the tumor microenvironment. For each tumor sample in this cohort, we purified malignant and stromal cells. We isolated immune cells (CD45+, EPCAM−), endothelial cells (CD31+, CD45−, EPCAM−), malignant cells (EPCAM+, CD45−), and fibroblasts (CD10+, CD45−, EPCAM−, CD31−), via flow cytometry as described elsewhere [14]. We performed RNA-seq for each cell type for every patient sample. We performed differential analysis on four cell types using SAM [22] to identify specific cell types in which the SUV_{max}-correlated genes were uniquely over-expressed with FDR less than 5%.

Tissue Microarray (TMA) Cohort

We examined the protein expression of GFPT2 (aka GFAT2) and glucose transporter SLC2A1 (aka GLUT1) by immunohistochemistry (IHC) using a NSCLC tissue microarray (n=211). With Institutional Review Board (IRB) approval in accordance with US Common Rule, patient samples were retrieved from surgical pathology archives at Department of Pathology, Stanford Medical Center [26]. SUV_{max} data was obtained from linked clinical database STRIDE. Of the 211 patients on the TMA, 52 AD patients had a ^{18}FDG-PET scan for which SUV_{max} was reported. The GFAT2 antibody was validated on controls as shown in Supplement 5 Figure S3. TMA staining intensity was assessed by qualitative ordinal scoring as 0 (negative), 1 (low), 2 (moderate), and 3 (high) for malignant cells and fibroblasts separately. An overall score was given to each sample based on the higher score between the malignant cells and fibroblasts. SUV_{max} was predicted using a general linear regression model based on staining scores for GFAT2 and GLUT1 as covariates. Survival analysis was performed using R “survival” package on all the AD patients using GFAT2 overall scores and fibroblast scores. Risk groups were defined by low GFAT2 expression (score 0 and 1) and high GFAT2 expression (score 2 and 3). Cox proportional hazard regression was used to obtain the p-value, hazard ratio (HR) and confidence interval (CI). A multivariate Cox model was used to obtain the prognostic significance of GFAT2 adjusted by age, stage, tumor size and gender.

TCGA NSCLC Cohort Analyses

Publicly available TCGA RNA-seq data on AD (n=511) and SCC (n=501) was used as an external cohort to verify DEGs between AD and SCC based on the RG cohort and to further analyze the relationship among genes correlated to glucose uptake identified in our RG cohort. TCGA gene expression profile was measured using Illumina HiSeq 2000 RNA-seq by the University of North Carolina genome characterization center, and RSEM normalized values were used for gene-level transcription estimates.

Copy number analysis—To identify potential genomic drivers of altered glucose uptake, we analyzed TCGA copy number variation (CNV) data of AD and SCC from UCSC Xena

[27]. CNV gene level data were processed by TCGA Firehouse pipeline [28,29]. In the UCSC Xena CNV data, 29 significant focal amplification and 46 significant focal deletion genomic regions were identified for AD, while 30 significant focal amplification and 53 significant focal deletion genomic regions were identified for SCC using GISTIC [30].

TGF-β-treated Cell Line Analyses

TGF-β-treated normal fibroblasts—To validate our findings in CAFs, we used the Affymetrix microarray gene expression dataset (GSE60880) [31] of normal fibroblast (NF) derived from normal human lung tissue treated with TGF-β. The NFs were incubated with TGF-β for 0.5, 1, 2 and 8 hours. CAF marker genes were used to assess the transformation of the NFs. We compared the expression of genes associated with glucose metabolism and SUV_{max} correlated genes enriched for EMT between the NFs and the CAF-like cells.

TGF-β-treated AD cell lines—To validate our findings on EMT, we analyzed the Affymetrix microarray gene expression dataset (GSE49644) [32] of three cell lines (A549, HCC827 and NCI-H358) before and after TGF-β treatment. Three replicates were included for each condition in each cell line. Replicates for each condition were normalized and merged for meta-analysis. Permutation multiple test (multtest) was applied to identify genes that changed significantly before and after induced EMT with FDR < 0.05. In particular, we investigated genes involved in glucose metabolism and SUV_{max} correlated genes functional enriched for EMT.

Western blot validation on HBP rate-limiting protein GFAT2 on TGF-β-treated AD—To investigate the relation between HBP rate-limiting gene GFPT2 (coding protein GFAT2) and EMT at protein level, we used western blots with human lung adenocarcinoma cells (HCC827). To induce EMT, cells were cultured in the presence of 2% FBS and 10 ng/ml TGF-β up to 10 days. Fresh media containing TGF-β was replenished every 2 days and cells were re-seeded if needed before reaching confluency. Levels of Histone H3 were used as an internal standard for equal loading. The blots were incubated with E-cadherin, Vimentin as well as GFAT2. Additional experimental details were included in Supplement 6.

Results

Differentially expressed genes reveal metabolic reprogramming differences by NSCLC histology

In our RG cohort, we identified 657 differentially expressed genes (DEGs) between AD and SCC (FDR<5%, Supplement 7). Genes more highly expressed in AD were enriched for processes related to extracellular matrix remodeling, whereas genes more highly expressed in SCC were enriched for cell growth and proliferation processes; these findings were validated in TCGA (Figure 1A, 1B and Supplement 8 Table S1). DEGs in glucose-driven metabolic pathways differed by histology (Figure 1C). SCC showed higher expressed DEGs in the glycolysis and pentose phosphate pathways (PPP), whereas AD showed higher expressed DEGs in the hexosamine biosynthesis pathway (HBP). Because SCC had higher SUV_{max} than AD (Supplement 9 Figure S4), we confirmed that the metabolic DEGs were histology specific and not reflective of differences in SUV_{max} (Supplement 9 Table S2).

Among metabolically-associated DEGs more highly expressed in SCC were: (i) SLC2A1 (FDR <0.0001), the glucose transporter I, (ii) G6PD (FDR= 0.0002), the gate-keeper gene of PPP, and (iii) PGD (FDR <0.0001), an indicator of higher production of NADPH, an essential reductant in anabolic reactions. These genes have been associated with cell proliferation and growth [33], supporting the Warburg effect. Among metabolically-associated DEGs more highly expressed in AD were: (i) GFPT1 (FDR <0.0001), the rate-limiting gene of HBP, and protein glycosylation genes (ii) OGT (FDR= 0.004) and (iii) GALE (FDR<0.0001); these genes suggest a unique role for HBP in AD that extends beyond the Warburg effect.

Glucose uptake is more associated with reactive stroma in AD than SCC

We identified genes correlated with SUV_{max} in AD and SCC samples separately from our RG cohort. In AD (n=96), 169 genes were correlated to glucose uptake (FDR<10%) (Supplement 10), of which 96 (57%) were found to be prognostic using PRECOG database (FDR<5%) [14]. Using WGCNA to cluster the 169 genes based on their bulk gene expression profiles in AD samples in our RG cohort, we obtained 6 gene clusters. We performed functional enrichment on each cluster in AD (Figure 2A), and we identified a gene cluster that was highly enriched for EMT (FDR= 3×10^{-38}). This particular cluster was also enriched for the extracellular matrix (FDR= 9×10^{-26}), suggesting a strong stromal factor. Interestingly, GFPT2, a rate-limiting gene in HBP, belonged to the gene cluster enriched for EMT and ECM. In SCC (n=31), 141 genes were correlated with SUV_{max} (FDR<20%), most of which were negatively correlated with SUV_{max} (Figure 2B and Supplement 11). Using WGCNA, we obtained 2 gene clusters based on bulk gene expression profiles in SCC samples. Functional enrichment analysis showed that SUV_{max}-correlated gene clusters in SCC were related to cell development (FDR = 6×10^{-3}) and chemical homeostasis (FDR = 4×10^{-5}). Among glucose-driven metabolic pathways in AD, we identified genes correlated to glucose uptake in the glycolysis pathway, including glucose transporter I (SLC2A1), PFKP, GAPDH and lactate transporter gene (SLC16A1) and GFPT2 (Figure 2C). Our findings were consistent with a previous study [19] that reported an association between increased glucose uptake and EMT in NSCLC based on bulk tumor gene expression and PET SUV_{max}; our findings extend the results of that study by showing that the association is histology specific and holds for AD, but not SCC.

In AD, among the genes correlated to glucose uptake, 55 genes were predominately expressed in a single cell-type of the tumor microenvironment: 25 in fibroblasts, 11 in immune, 17 in malignant cells, and 2 in endothelial cells, and several were shared across multiple compartments (Figure 3A). Of the 55 AD genes predominately expressed in a single cell-type, 30 were prognostically significant, including GFPT2 (PRECOG, FDR<5%). The vast majority of these prognostically significant genes were secreted factors (Supplement 10), likely facilitating cell-cell crosstalk associated with disease progression. In SCC, 28 genes correlated to glucose uptake were largely confined to the malignant compartment (Figure 3B), suggesting that glucose uptake is more associated with a reactive stromal in AD than SCC.

GFPT2-expressing CAFs are associated with glucose uptake and prognostically significant in AD, as validated in an independent tissue microarray (TMA) cohort

In our study, GFPT2 was the only prognostically significant gene in AD correlated to glucose uptake which was predominately expressed in a single stromal compartment and associated with a glucose-driven metabolic pathway (Supplement 10). We confirmed the prognostic significance of GFPT2 in TCGA (p-value=0.002, HR=1.27,CI=[1.1,1.5]) for AD. Interestingly, GFPT2, a rate-limiting gene of HBP, showed the strongest expression in CAFs (Figure 3C). To confirm the CAF enrichment of this sorted subpopulation in our TME cohort, we verified that this cell subpopulation uniquely over-expressed common CAF marker genes (ACTA2, FAP, FGF1, PDGFRB, COL1A1 and FN1) (Figure 3D). In TCGA, GFPT2 expression was strongly correlated to secreted glycoproteins that were also correlated to glucose uptake (Figure 4A); many of these genes coding these glycoproteins are expressed by the CAF compartment in our TME cohort and were associated with EMT and extracellular matrix (ECM). This finding is consistent with previous study that showed EMT could induce aberrant glycosylation through HBP activation [34].To validate the role of GFPT2 in EMT, we showed that at the protein level, GFAT2 (GFPT2 coded protein) increased in AD cells following TGF-β induced EMT (Figure 4B).

We validated the GFPT2-SUV_{max} association in CAFs in an external cohort based on TMA (Figure 5A). We found that the TMA overall scores of protein GFAT2 (coded by GFPT2 gene) expression were predictive of SUV_{max}. Moreover, in the TMA, we observed that CAFs were more likely to express GFAT2 than malignant cells, but if malignant cells expressed GFAT2 then GFAT2 was expressed in the CAFs at a similar or higher level. Because glucose uptake is commonly associated with GLUT1 (SLC2A1) expression, we evaluated the predictive significance of both GLUT1 and GFAT2 for SUV_{max}. Interestingly, GFAT2 in CAFs alone and GLUT1 in malignant cells were both predictive of SUV_{max} (Supplement 12 Figure S5). A side-by-side comparison of GLUT1 and GFAT2 in a representative TMA sample with high SUV_{max} showed GLUT1 confined to the malignant cells and GFAT2 to the fibroblasts (Figure 5B). A representative case from our RG cohort with relatively high SUV_{max} expression showed that the GFPT2-expressing CAFs were located at the invasive edge of the tumor (Figure 5C). We also found that GFAT2 scores overall and fibroblasts only were highly prognostic among AD patients in the TMA cohort (n=211) adjusted for age, stage, tumor size and sex (Figure 5D and Supplement 12 Table S3). In particular, prognostic significance of GFAT2 fibroblast score implicates the importance of reactive stromal as a potential therapeutic target for AD.

In several of our TMA samples, we also found GFAT2 expressed in the malignant cells. To investigate the genomic significance of this finding, we observed that GFPT2 gene is located on chromosome 5q region that was recurrently amplified in TCGA AD, but recurrently deleted in TCGA SCC (Supplement 13 Figure S6). Interestingly, numerous genes correlated to glucose uptake are located in the same genomic region, including VCAN, coding extracellular matrix protein versican, and TGFBI and FBN2 that are both related to TGF-β signaling, a signaling pathway known to play an important role in EMT [35].

TGF-β induction of EMT and CAF-like phenotypes are associated increased GFPT2

Because GTPF2 is a known driver of HBP and HBP has been associated with EMT, we hypothesized that GFPT2 expression would increase with TGF-β treatment in both normal fibroblasts (NFs) and malignant cells. Our rationale was based on the observations that TGF-β transforms NF to CAF-like cells and induces EMT in AD. We found TGFBI, known to be induced by TGF-β, was also correlated to glucose uptake (Supplement 10). We investigated expression of glucose metabolism genes and EMT-genes associated with glucose uptake in human lung NFs before and after TGF-β treatment (GSE60880). Following TGF-β treatment, the NFs were transformed to CAF-like cells based on the gene expression of common CAF markers (Supplement 14 Figure S7). Consistent with our hypothesis, the HBP genes were more expressed in the CAF-like cells than the NFs (Figure 6A); in comparison, there were little to no change in genes related to glycolysis, PPP and TCA cycle, suggesting no change in genomic regulation of these metabolic pathways with the transformation of NF to CAF-like cells. Also, many EMT-genes associated with glucose uptake were upregulated in the CAF-like cells (Figure 6A).

With TGF-β treatment, NSCLC AD cell lines (GSE49644) have been shown to undergo EMT. We analyzed this transformation in terms of changes in glucose metabolism related genes and EMT-genes correlated to glucose uptake. We found that glucose metabolism genes associated with energy production and cell proliferation (glycolysis, PPP, TCA cycle) were mostly unchanged or reduced after TGF-β induced EMT, whereas several HBP genes and most EMT-genes correlated glucose uptake were increased (Figure 6B). This is consistent with our prior observation that GFAT2 (GFPT2 coded protein) increased AD cells following TGF-β induced EMT (Figure 4B).

In parallel to the cell line analyses, we analyzed expression of the metabolic genes and the EMT-genes associated with glucose uptake across the different cell-specific compartments of AD in our TME cohort, we found metabolic genes associated with energy production and cell proliferation (glycolysis, PPP, TCA cycle) were strongly expressed in malignant cells, whereas HBP and EMT-genes associated with glucose uptake were mostly expressed among the CAFs (Figure 6C). Taken together, these findings indicate that altered glucose metabolism in tumor stroma through HBP is related to processes associated with EMT, possibly facilitating cancer invasion.

Discussion

The best-characterized metabolic behavior of cancer is the Warburg effect, however, tumor metabolic reprogramming is not restricted to support tumor growth and proliferation, and it is not restricted to malignant cells. In this analysis, we provided evidence of metabolic reprogramming in the tumor stroma of AD that is prognostically significant. We applied a radiogenomic analysis, which integrated data on glucose uptake, as measured on ^{18}FDG-PET scans, and transcriptomics of the bulk and flow-sorted human tumors. Our analysis revealed surprising differences in glucose metabolism between AD and SCC, the two major histological subtypes of NSCLC. Compared to AD, SCC had more highly expressed genes in glycolysis and pentose phosphate pathways, which are associated with Warburg effect, whereas AD had more highly expressed genes in the HBP, which have not been associated

with the Warburg effect. For AD, genes correlated to glucose uptake were enriched for EMT and ECM. The glucose uptake and EMT was previously reported in NSCLC on the first 26 patients of our RG cohort [19], but we found it held only for AD, not SCC, given the larger size of current RG cohort (n=130). For SCC, genes associated with glucose uptake were functionally enriched for tumor growth. Using cell-type-specific transcriptomics of the NSCLC TME, we found a stronger association of altered glucose uptake in the tumor stroma of AD compared to that of SCC. Taken together, our analysis confirmed a prior report that metabolic reprogramming in NSCLC is histology-specific [13] and extended this finding to show that the molecular pathways and cell-types associated with glucose uptake were also histology-specific.

We explored the significance of GFPT2 as a mediator of tumor metabolic programming in the stromal compartment of AD and a predictor of survival outcomes. GFPT2 was found to be prognostically significant in PRECOG, TCGA and our TMA cohort for AD. GFPT2 and its isoform, GFPT1, are both rate limiting genes of HBP, however they have significant differences. GFPT1 is expressed in many cell types, but GFPT2 expression is thought to be more restricted to specific cell types [36]. In a pathological context, GFPT2 has been associated with diabetes, with few reports relevant to cancer, whereas GFPT1 has been well studied in the context of both diabetes and cancer [37]. In our analysis, we found GFPT1 was more highly expressed in AD relative to SCC, but GFPT2 was correlated to glucose uptake in AD, suggesting that GFPT2 (not GFPT1) is associated with AD progression. We validated the correlation of GFPT2 and SUV_{max} on TMA of AD. The TMA also supported our finding that GFPT2 is largely expressed in CAFs but GFPT2 can be expressed in malignant cells. Because it was not common to find GFPT2-expressing malignant cells in the absence of GFPT2-expressing in CAFs, it is possible that GFPT2 expression in CAFs may be a precursor to GFPT2 expression in malignant cells for AD. Also, because GFPT2 is recurrently amplified in AD and deleted in SCC, AD may have a genomic propensity toward the HBP through GFPT2 among the malignant cells.

In AD, when we jointly analyzed SLC2A1 (GLUT1) expression in malignant cells and GFPT2 expression in CAFs, we found that GFPT2 expression in CAFs was an independent predictor of SUV_{max}, suggesting that the GFPT2-expressing CAFs may have increased glucose uptake. Prior work has shown that when NFs were transformed to CAF-like cells, through TGF-β treatment, glucose uptake increased [38]. Interestingly, we did not observe any changes in the expression of GLUT1 when comparing NF and CAFs. Moreover we did not observe significant GLUT1 expression in CAFs on TMA, even at the high SUV levels (analysis not shown). It is possible that glucose uptake in the CAFs may be altered through other regulatory mechanisms. We did observe that the insulin-regulatory gene IGFBP5 was correlated to glucose uptake and uniquely expressed in CAFs (Supplement 10), suggesting that it may have a role in regulating glucose uptake [39].

Our findings on GFPT2 and the HBP provide an important link between altered metabolic reprogramming and altered cellular signaling in AD. HBP uses glycolytic intermediates to generate UDP-GlcNAc and UDP-GalNAc which serve as the substrates for biosynthesis of glycoproteins, including many associated with promoting EMT and cancer invasion [40]. For example, elevated O-glycosylated fibronectin (FN1) could induce EMT in human lung

carcinoma cells [41]; in our analysis, FN1 was among the genes correlated with glucose uptake and uniquely expressed by CAFs and one of many EMT- genes associated glucose uptake. Interestingly, because only 2–5% of glucose is typically shunted to the HBP [42], it is possible that a small absolute increase of glucose to the HBP could represent a large percentage change for HBP and have a dramatic effect. Moreover, if small changes in glucose flux to the HBP promote invasion this could explain why AD has poorer prognosis for lower overall levels of glucose uptake compared to SCC. Understanding the impact of small alterations in glucose uptake to the HBP through carbon-labeled glucose flux analysis, in both the malignant and stromal compartment of tumors, promises to provide new insights into tumor metabolic reprogramming beyond the Warburg effect.

While our study provides new insights with respect to tumor metabolic behavior, it has its limitations. First, the sample size of SCC in our RG cohort was small (n=31), therefore, our SUV_{max}-gene correlation analysis in SCC had relatively large false discovery rate. This limited our ability to identify statistically significant genes in SCC that could be driving glucose metabolic alterations and cellular processes. Despite this limitation, we can conclude that the SCC likely does not involve EMT-SUV_{max} correlated genes because when we repeatedly subsampled the AD cases to match the sample size of the SCC cases, we still found the EMT association held with a p-value < 5% in AD (analysis not shown). Second, our analysis was limited to genes associated with maximum SUV, but other features of glucose uptake measured on PET, such as the total lesion glycolysis (TLG) and SUV variation, are worthy of pursuit and may reveal additional insights [18]. Third, on our TME cohort, the malignant cells were restricted to the EPCAM-positive subpopulation, and thus a more mesenchymal malignant cell type might be lost that could exhibit a higher expression of GFPT2 as found in TGF-β-induced EMT in AD (Figure 4B). Moreover, because it has been shown that tumor cells that undergo EMT downregulate EPCAM and upregulate CD10 [43,44], our CAFs sorted based on CD10+, CD45−, EPCAM− and CD31− markers could potentially include mesenchymal malignant cells, although that is any contamination by malignant cells seems minimal because our CAFs express canonical CAF markers (Figure 3D). Finally, the TMA analysis was limited to 6mm. Further analysis of whole slide images would provide a more comprehensive assessment of GFPT2 spatial distribution in the TME.

Our work highlighted CAFs as a major contributor to the metabolic reprogramming of the TME in AD, however the endothelial and immune cells were also implicated in our analysis and deserve consideration going forward. Much of our focus was on GFPT2 but our analysis provided many more SUV_{max}-associated genes that deserve further exploration. We focused on GFPT2 because it is a metabolic enzyme that has been underreported in the cancer context. Its relevance in AD suggests that GFPT2 deserves more consideration in cancers and possibly beyond its role in the HBP. Our work provides a spotlight on the HBP for promoting tumor invasion in AD and may explain why the lower glucose uptake for AD relative to SCC carries worse prognosis. A more in-depth analysis of this behavior is warranted. Finally, our findings have therapeutic implications, suggest that hexosamine biosynthesis pathway and glycosylation inhibitors (such as ST060266 and Tunicamycin [37]) could be effective for AD, whereas, SCC may be more effectively targeted by pentose phosphate pathway and glycolytic inhibitors (such as 6-AN and 2-DG [45]).

In summary, our integrative analysis showed that glucose uptake associated with GFPT2-expressing CAFs was prognostic for AD. In SCC, glucose uptake was associated with glycolysis and higher proliferation potential. In AD, we found a stromal component to glucose uptake implicating CAFs, endothelial and immune cells. In AD, we focused our analysis on GFPT2 and its relation to hexosamine biosynthesis pathway that could bridge the altered glucose metabolism with protein glycosylation. These insights can provide a therapeutic approach for targeting tumor-stromal interactions associated with disease progression by disrupting the unique metabolic tumor microenvironment of AD.

Supplementary Material

Refer to Web version on PubMed Central for supplementary material.

Acknowledgments

We are grateful to Dr. Ann Leung for providing a valuable review of our manuscript.

Funding: The work was supported by the National Institutes of Health (NIH) grants R01 CA160251 and U01 CA154969.

References

1. Warburg O. The metabolism of carcinoma cells. J Cancer Res. 1925; 9(1):148–163.
2. Ward PS, Thompson CB. Metabolic reprogramming: A cancer hallmark even Warburg did not anticipate. Cancer Cell. 2012; 21(3):297–308. [PubMed: 22439925]
3. Hanahan D, Weinberg RA. Hallmarks of cancer: The next generation. Cell. 2011; 144(5):646–674. [PubMed: 21376230]
4. Zhang B, Zheng A, Hydbring P, Ambroise G, Ouchida AT, Goiny M, et al. PHGDH defines a metabolic subtype in lung adenocarcinomas with poor prognosis. Cell Reports. 2017; 19(11):2289–2303. [PubMed: 28614715]
5. Hensley CT, Faubert B, Yuan Q, Lev-Cohain N, Jin E, Kim J, et al. Metabolic heterogeneity in human lung tumors. Cell. 2016; 164(4):681–694. [PubMed: 26853473]
6. Gupta S, Roy A, Dwarakanath BS. Metabolic cooperation and competition in the tumor microenvironment: Implications for therapy. Front Oncol. 2017; 7:1–24. [PubMed: 28168163]
7. Martinez-Outschoorn UE, Lin Z, Trimmer C, Flomenberg N, Wang C, Pavlides S, et al. Cancer cells metabolically “fertilize” the tumor microenvironment with hydrogen peroxide, driving the Warburg effect: Implications for PET imaging of human tumors. Cell Cycle. 2011; 10(15):2504–2520. [PubMed: 21778829]
8. Pértega-Gomes N, Vizcaíno JR, Attig J, Jurmeister S, Lopes C, Baltazar F. A lactate shuttle system between tumour and stromal cells is associated with poor prognosis in prostate cancer. BMC Cancer. 2014; 14(1):352. [PubMed: 24886074]
9. Siegel RL, Miller KD, Jemal A. Cancer statistics. CA Cancer J Clin. 2016; 66(1):7–30. [PubMed: 26742998]
10. Pikor LA, Ramnarine VR, Lam S, Lam WL. Genetic alterations defining NSCLC subtypes and their therapeutic implications. Lung Cancer. 2013; 82(2):179–189. [PubMed: 24011633]
11. Zhang L, Wang L, Du B, Wang T, Tian P, Tian S. Classification of non-small cell lung cancer using significance analysis of microarray gene set reduction algorithm. Biomed Res Int. 2016
12. Kuner R, Muley T, Meister M, Ruschhaupt M, Buness A, Xu EC, et al. Global gene expression analysis reveals specific patterns of cell junctions in non-small cell lung cancer subtypes. Lung Cancer. 2009; 63(1):32–38. [PubMed: 18486272]
13. Schuurbiers OC, Meijer TW, Kaanders JH, Looijen-Salamon MG, deGeus-Oei LF, van der Drift MA, et al. Glucose metabolism in NSCLC is histology-specific and diverges the prognostic

potential of ^{18}FDG-PET for adenocarcinoma and squamous cell carcinoma. J Thorac Oncol. 2014; 9(10):1485–1493. [PubMed: 25170642]

14. Gentles AJ, Newman AM, Liu CL, Bratman SV, Feng W, Kim D, et al. The prognostic landscape of genes and infiltrating immune cells across human cancers. Nat Med. 2015; 21(8):938–945. [PubMed: 26193342]
15. Ogata H, Goto S, Sato K, Fujibuchi W, Bono H, Kanehisa M. KEGG: Kyoto encyclopedia of genes and genomes. Nucleic Acids Res. 1999; 27(1):29–34. [PubMed: 9847135]
16. Romero P, Wagg J, Green ML, Kaiser D, Krummenacker M, Karp PD. Computational prediction of human metabolic pathways from the complete human genome. Genome Biol. 2005; 6(1):R2. [PubMed: 15642094]
17. Hay N. Reprogramming glucose metabolism in cancer: can it be exploited for cancer therapy? Nat Rev Cancer. 2016; 16(10):1–15. [PubMed: 26612535]
18. Nair VS, Gevaert O, Davidzon G, Napel S, Graves EE, Hoang CD, et al. Prognostic PET 18F-FDG uptake imaging features are associated with major oncogenomic alterations in patients with resected non-small cell lung cancer. Cancer Res. 2012; 72(15):3725–3734. [PubMed: 22710433]
19. Yamamoto S, Huang D, Du L, Korn RL, Jamshidi N, Burnette BL, et al. Radiogenomic analysis demonstrates associations between (18)F-Fluoro-2-Deoxyglucose PET, prognosis, and epithelial-mesenchymal transition in non-small cell lung cancer. Radiology. 2016; 280(1):261–270. [PubMed: 27082783]
20. Johnson WE, Li C, Rabinovic A. Adjusting batch effects in microarray expression data using empirical Bayes methods. Biostatistics. 2007; 8(1):118–127. [PubMed: 16632515]
21. Pollard KS, Birkner MD, Van Der Laan MJ, Dudoit S. Test statistics null distributions in multiple testing: Simulation studies and applications to genomics. 2005
22. Tusher VG, Tibshirani R, Chu G. Significance analysis of microarrays applied to the ionizing radiation response. Proc Natl Acad Sci U S A. 2001; 98(9):5116–5121. [PubMed: 11309499]
23. Langfelder P, Horvath S. WGCNA: An R package for weighted correlation network analysis. BMC Bioinformatics. 2008; 9:559. [PubMed: 19114008]
24. Subramanian A, Tamayo P, Mootha VK, Mukherjee S, Ebert BL, Gillette MA, et al. Gene set enrichment analysis: A knowledge-based approach for interpreting genome-wide expression profiles. Proc Natl Acad Sci U S A. 2005; 102(43):15545–15550. [PubMed: 16199517]
25. Chen J, Bardes EE, Aronow BJ, Jegga AG. ToppGene Suite for gene list enrichment analysis and candidate gene prioritization. Nucleic Acids Res. 2009; 37(SUPPL. 2):305–311.
26. Nair VS, Gevaert O, Davidzon G, Plevritis SK, West R. NF-κB protein expression associates with 18F-FDG PET tumor uptake in non-small cell lung cancer: A radiogenomics validation study to understand tumor metabolism. Lung Cancer. 2014; 83(2):189–196. [PubMed: 24355259]
27. UCSC Xena. [Accessed January 4, 2017] http://xena.ucsc.edu/
28. [Accessed January 4, 2017] SNP6 Copy number analysis (GISTIC2) - Lung Adenocarcinoma (Primary solid tumor). http://gdac.broadinstitute.org/runs/analyses__2016_01_28/reports/cancer/LUAD-TP/CopyNumber_Gistic2/nozzle.html
29. [Accessed January 4, 2017] SNP6 Copy number analysis (GISTIC2) - Lung Squamous Cell Carcinoma (Primary solid tumor). http://gdac.broadinstitute.org/runs/analyses__2016_01_28/reports/cancer/LUSC-TP/CopyNumber_Gistic2/nozzle.html
30. Mermel CH, Schumacher SE, Hill B, Meyerson ML, Beroukhim R, Getz G. GISTIC2.0 facilitates sensitive and confident localization of the targets of focal somatic copy-number alteration in human cancers. Genome Biol. 2011; 12(4):R41. [PubMed: 21527027]
31. Glyn Bradley. [Accessed January 18, 2017] GSE60880. https://www.ncbi.nlm.nih.gov/geo/query/acc.cgi?acc=GSE60880
32. Sun Y, Daemen A, Hatzivassiliou G, Arnott D, Wilson C, Zhuang G, et al. Metabolic and transcriptional profiling reveals pyruvate dehydrogenase kinase 4 as a mediator of epithelial-mesenchymal transition and drug resistance in tumor cells. Cancer Metab. 2014; 2(1):20. [PubMed: 25379179]
33. Jiang P, Du W, Wu M. Regulation of the pentose phosphate pathway in cancer. Protein Cell. 2014; 5(8):592–602. [PubMed: 25015087]

34. Lucena MC, Carvalho-Cruz P, Donadio JL, Oliveira IA, de Queiroz RM, Marinho-Carvalho MM, et al. Epithelial mesenchymal transition induces aberrant glycosylation through hexosamine biosynthetic pathway activation. J Biol Chem. 2016; 291(25):12917–12929. [PubMed: 27129262]
35. Xu J, Lamouille S, Derynck R. TGF-β-induced epithelial to mesenchymal transition. Cell Res. 2009; 19(2):156–172. [PubMed: 19153598]
36. McKnight GL, Mudri SL, Mathewes SL, Traxinger RR, Marshall S, Sheppard PO, et al. Molecular cloning, cDNA sequence, and bacterial expression of human glutamine:fructose-6-phosphate amidotransferase. J Biol Chem. 1992; 267(35):25208–25212. [PubMed: 1460020]
37. Vasconcelos-dos-Santos A, Oliveira IA, Lucena MC, Mantuano NR, Whelan SA, Dias WB, et al. Biosynthetic machinery involved in aberrant glycosylation: Promising targets for developing of drugs against cancer. Front Oncol. 2015; 5:138. [PubMed: 26161361]
38. Andrianifahanana M, Hernandez DM, Yin X, Kang JH, Jung MY, Wang Y, et al. Profibrotic up-regulation of glucose transporter 1 by TGF-β involves activation of MEK and mammalian target of rapamycin complex 2 pathways. FASEB J. 2016; 30(11):3733–3744. [PubMed: 27480571]
39. Song SE, Kim YW, Kim JY, Lee DH, Kim JR, Park SY. IGFBP5 mediates high glucoseinduced cardiac fibroblast activation. J Mol Endocrinol. 2013; 50(3):291–303. [PubMed: 23417767]
40. Taparra K, Tran PT, Zachara NE. Hijacking the hexosamine biosynthetic pathway to promote EMT-mediated neoplastic phenotypes. Front Oncol. 2016; 6:85. [PubMed: 27148477]
41. Ding Y, Gelfenbeyn K, Freire-De-Lima L, Handa K, Hakomori SI. Induction of epithelial-mesenchymal transition with O-glycosylated oncofetal fibronectin. FEBS Lett. 2012; 586(13): 1813–1820. [PubMed: 22641031]
42. Buse MG. Hexosamines, insulin resistance and the complications of diabetes: current status. Am J Physiol Endocrinol Metab. 2006; 290(1):E1–E8. [PubMed: 16339923]
43. Sankpal NV, Fleming TP, Sharma PK, Wiedner HJ, Gillanders WE. A double-negative feedback loop between EpCAM and ERK contributes to the regulation of epithelial-mesenchymal transition in cancer. Oncogene. 2017; 36:3706–3717. [PubMed: 28192403]
44. Lee KW, Sung CO, Kim JH, Kang M, Yoo HY, Kim HH. CD10 expression is enhanced by Twist1 and associated with poor prognosis in esophageal squamous cell carcinoma with facilitating tumorigenicity in vitro and in vivo. Int J. Cancer. 2015; 136(2):310–321. [PubMed: 24895167]
45. Pelicano H, Martin DS, Xu RH, Huang P. Glycolysis inhibition for anticancer treatment. Oncogene. 2006; 25(34):4633–4646. DOI: 10.1038/sj.onc.1209597 [PubMed: 16892078]

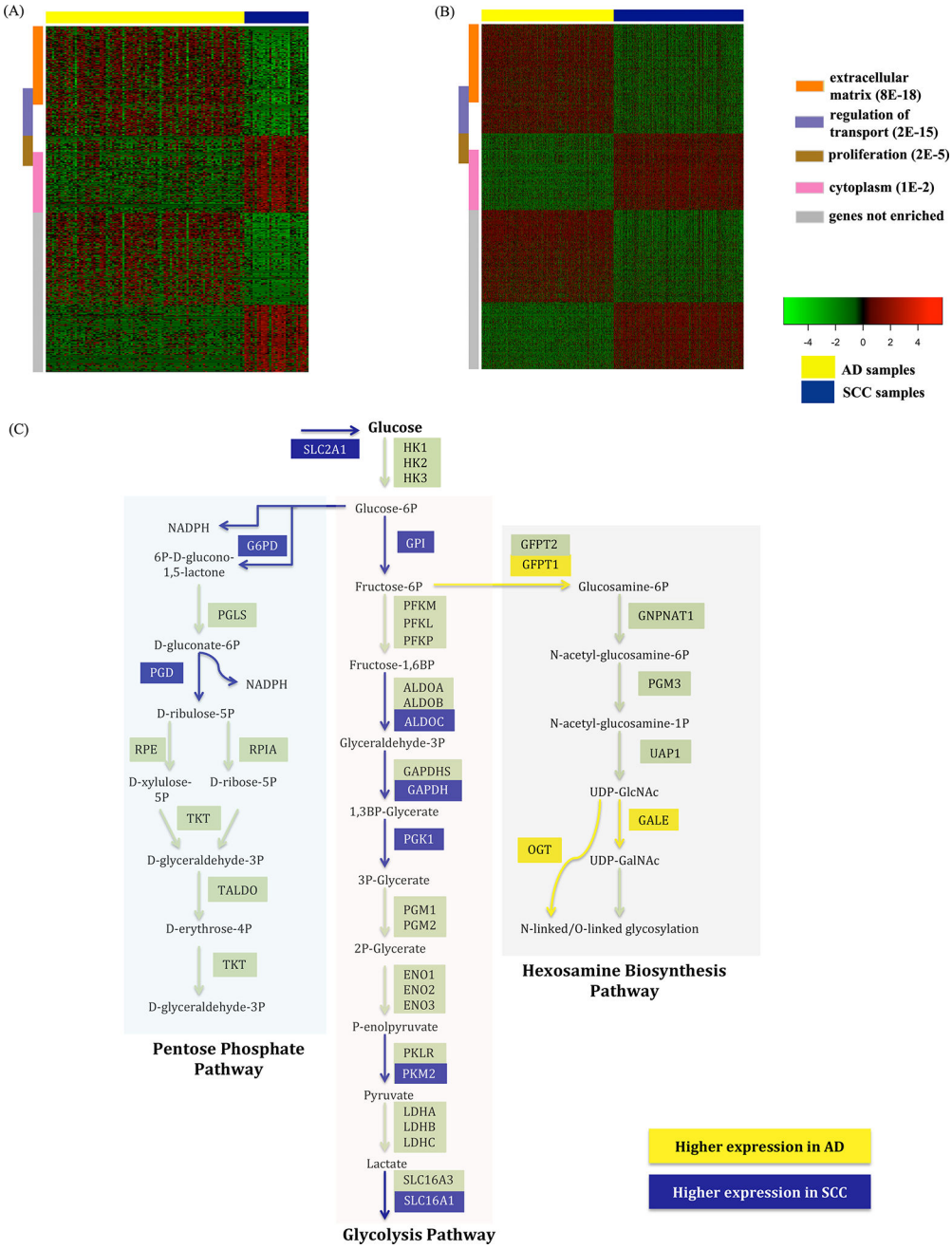

Figure 1.

Differentially expressed genes (DEGs) between AD and SCC. **(A)** Heatmap of DEGs between AD and SCC in the radiogenomics (RG) cohort. **(B)** Heatmap for TCGA showing only the DEGs derived from the radiogenomics cohort. Yellow denotes AD, and Blue denotes SCC samples. DEGs are annotated for enrichment of extracellular matrix (coral), regulation of transport related to invasion (lavender), proliferation (brown), cytoplasm (pink), or unassigned (grey). The enrichment FDRs are shown in parenthesis. **(C)** Glucose-driven metabolic pathways: glycolysis, pentose phosphate pathway and hexosamine biosynthesis pathway. All DEGs in the glucose metabolic pathways were differentially

expressed in both RG cohort and TCGA, except for G6PD and PKM2 which were only differentially expressed in TCGA, and OGT which was only differentially expressed in the RG cohort.

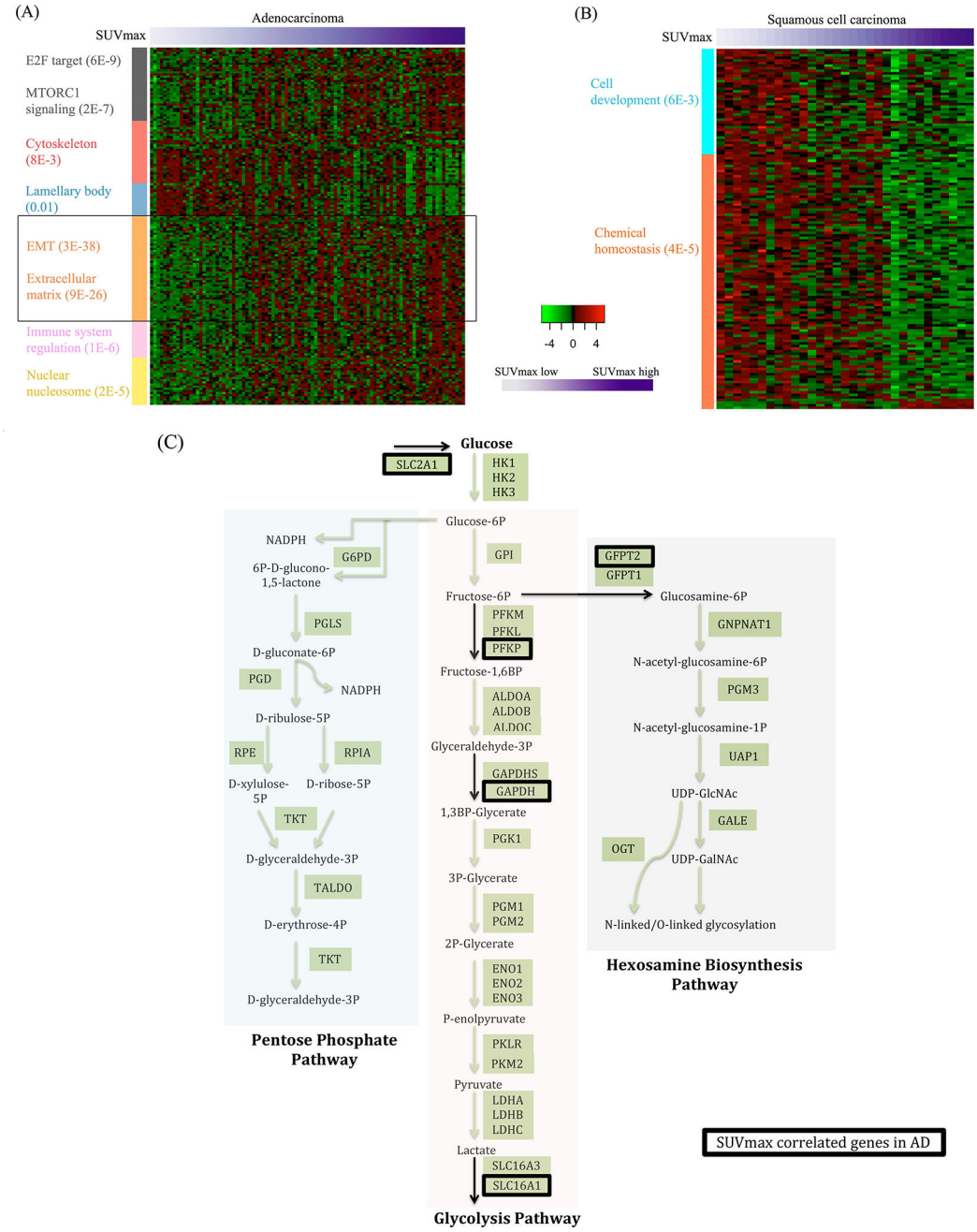

Figure 2.

Heatmap of SUV_{max} correlated genes in Adenocarcinomas **(A)** and Squamous cell carcinomas **(B)** in the radiogenomics (RG) cohort. FDRs for functional enrichment are indicated in parenthesis. Patients (columns) are sorted from low SUV_{max} to high SUV_{max}. **(C)** Glucose metabolism genes that are correlated to glucose uptake in AD samples in the RG cohort.

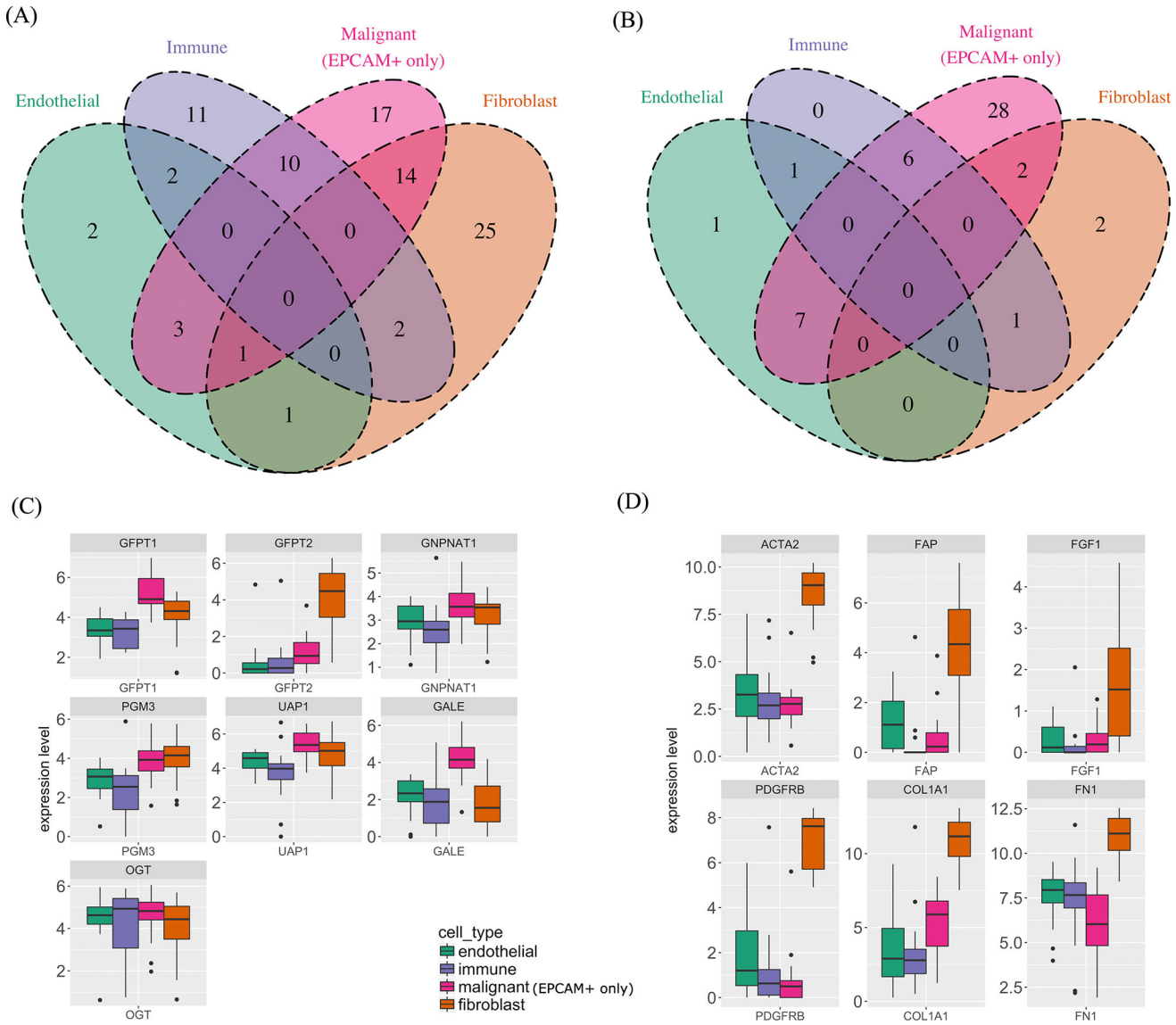

Figure 3.

Analysis of genes associated with glucose metabolic reprogramming in the tumor microenvironment. **(A)** For AD, genes correlated with glucose uptake are placed on Venn diagram by cell-type-specific expression (derived from TME cohort), showing the largest number of uniquely expressed genes are in fibroblasts. **(B)** For SCC, genes correlated with glucose uptake are placed on Venn diagram by cell-type-specific expression (derived from TME cohort), showing the largest number of uniquely expressed genes are in the malignant cells, with few genes expressed in other cell-types. **(C)** Expression of HBP genes in the four cell-types (TME cohort, AD samples), showing fibroblasts and malignant cells have higher expression of HBP genes than immune and endothelial cells. **(D)** Expression of common CAF marker genes in the four cell types in the (TME cohort, AD samples), confirming the expected behavior of the CAF subpopulation.

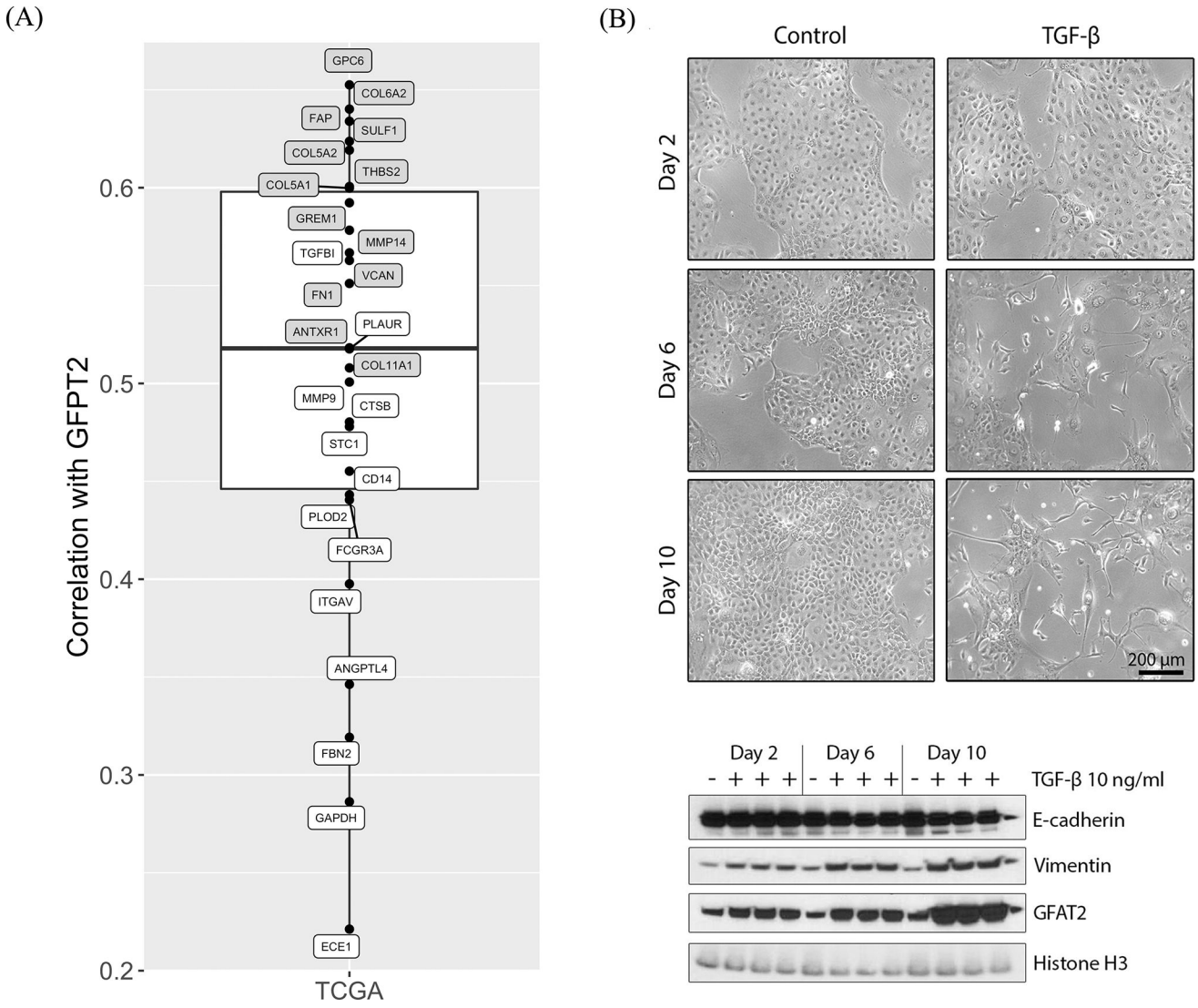

Figure 4.

Validation of association of GFPT2 and SUV_{max}-associated secreted glycoproteins and EMT. **(A)** Correlation between GFPT2 and glycoprotein-coding genes correlated with glucose uptake in TCGA AD. Genes highlighted in gray were more expressed in CAFs compared to other cells in our TME cohort; these genes are among highest correlated. **(B)** Morphological and protein expression changes in HCC827 cells after EMT induction with TGF-β treatment. (Top) Phase-contrast microscopy showing HCC827 cells after treatment with, or without (control), TGF-β (10 ng/ml) up to 10 days. All images were obtained at a magnification of 100×. Scale bar represents 200 μm. (Bottom) Following TGF-β treatment on HCC827, protein lysates were harvested at the indicated time points and E-cadherin, Vimentin and Glutamine fructose-6-phosphate amidotransferase 2 (GFAT2: protein coded by GFPT2 gene) were analyzed by Western blot. Histone H3 was used an internal loading control. During the EMT time course, Vimentin increased, E-cadherin decreased and GFAT2 increased.

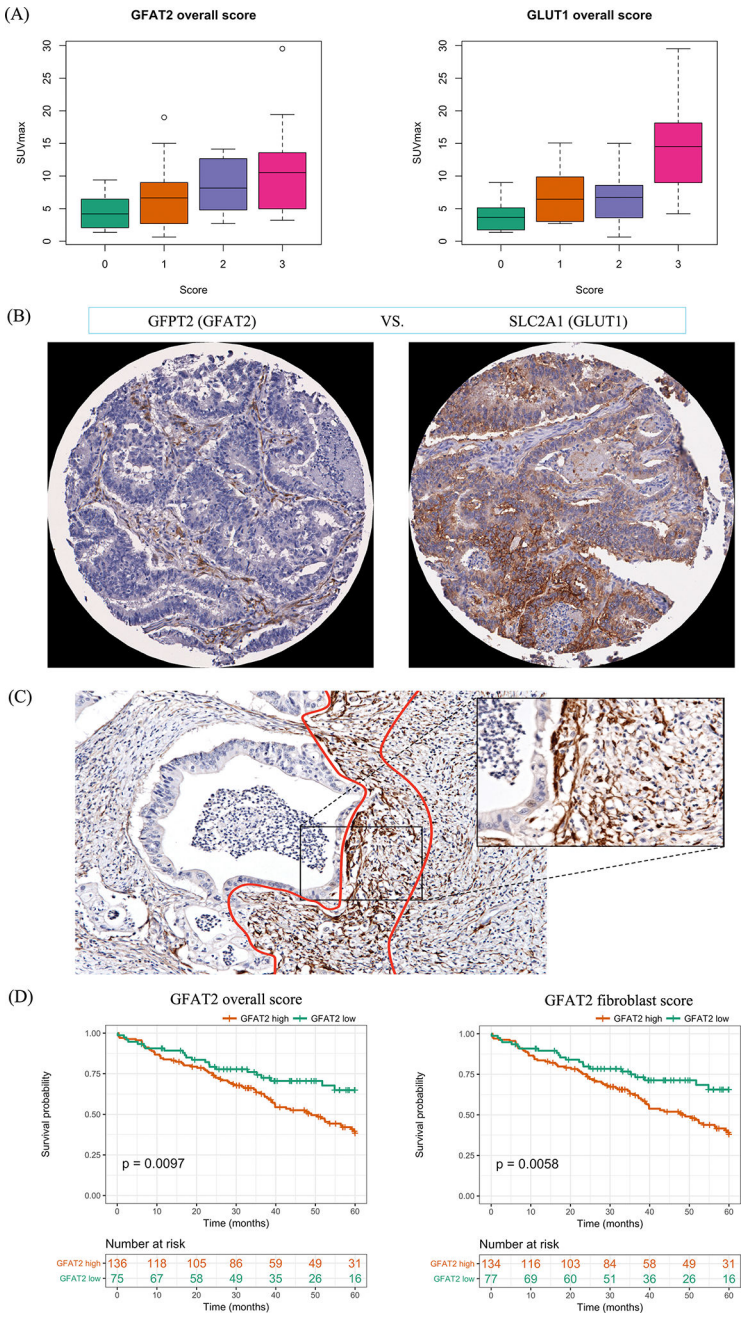

Figure 5.

Validation of the correlation between GFPT2 and SUV_{max} in TMA cohort and survival analysis based on GFAT2 protein. **(A)** Statistically significant correlation between GFAT2 (coded by GFPT2 gene) and GLUT1 (SLC2A1) with SUV_{max} (GFAT2 p-value: 0.003, GLUT1 p-value: 0.005). **(B)** Representative sample from TMA of paired GFAT2 and GLUT1 expression, illustrating GFAT2 expression localization to fibroblasts and simultaneous GLUT1 expression localization to malignant cells. **(C)** Representative whole slide microphotograph of GFAT2 expression showing GFAT2 enriched in cancer-associated fibroblasts at tumor periphery. **(D)** GFAT2 staining overall and fibroblast scores were both

prognostic for 5-year survival in TMA adenocarcinoma patients. Overall score: p-value=0.0097, HR=1.86, CI=[1.15, 2.99]. Fibroblast score: p-value=0.0058, HR=2.05, CI=[1.20, 3.11].

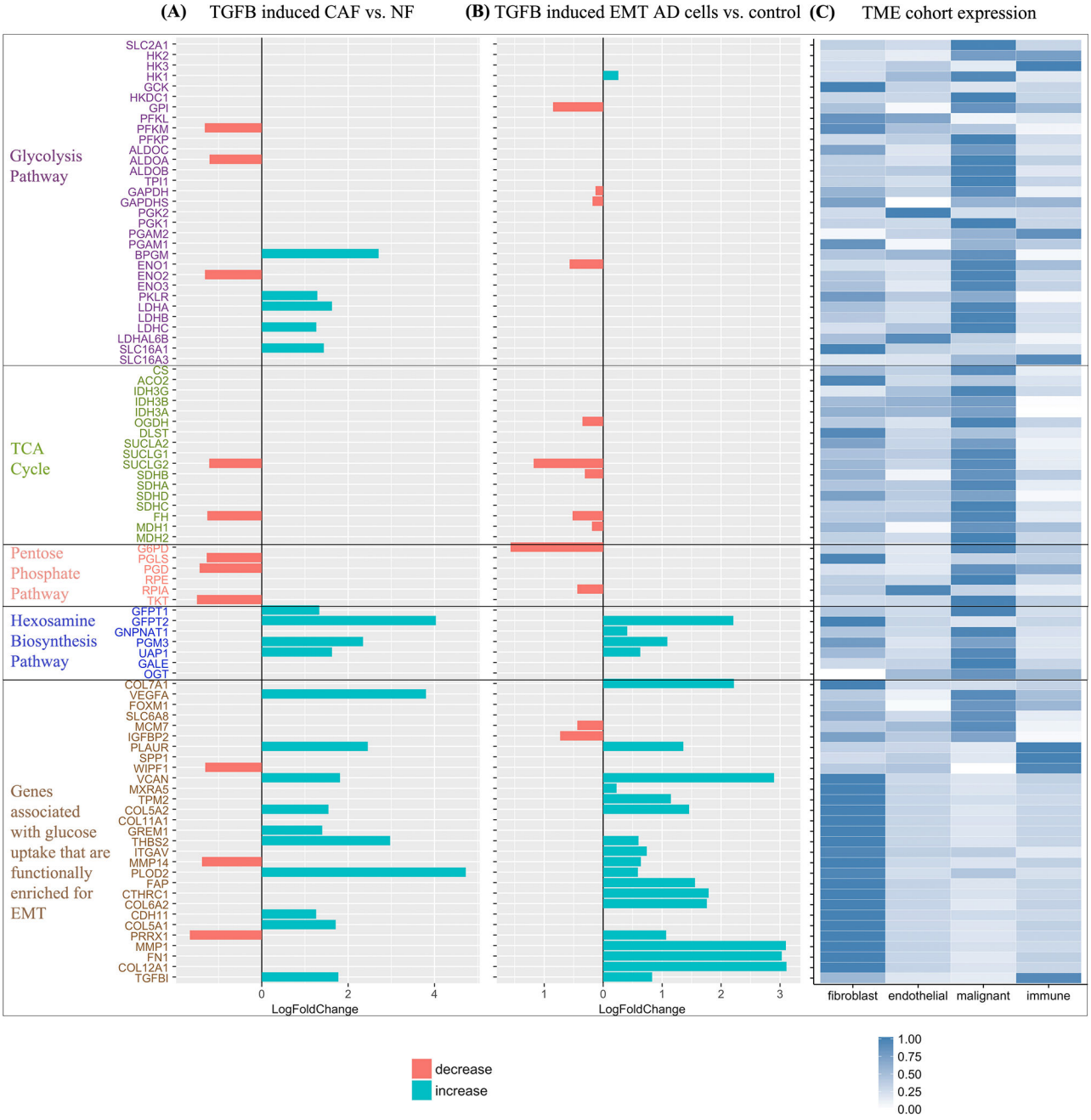

Figure 6.

Glucose metabolism related genes and genes associated with glucose uptake that are functionally enriched for EMT in the validation cell line data and TME cohort. **(A)** TGF-β induced cancer-associated fibroblast (CAF) compared to normal fibroblast (NF) (GSE60880). **(B)** AD cell lines with TGF-β induced EMT compared to AD cell lines without TGF-β treatment (control) (GSE49644). **(C)** Heatmap of normalized average expression of the genes in each of the four cell types in the TME cohort AD samples.

Table 1

Overview of patient demographics of various cohorts that contributed to this analysis.

Variable	RG	TME	TCGA	TMA
Number of patients	130	40[a]	1012	211[b]
Age (mean, standard deviation)	(69, 9)	(68, 13)	NA[c]	(67, 11)
Gender				
Male	96	25	606	85
Female	34	8	406	126
Histology				
Adenocarcinoma	96	20	511	211
Squamous cell carcinoma	31	11	501	0
Undefined	3	2	0	0
Stage				
Stage I	74	12	522	108
Stage II	30	14	286	60
Stage III	19	6	168	41
Stage IV	4	0	33	2
Undefined	3	1	3	0
Median follow-up (months)	22	16	8	38
Number of deaths	27	4	283	108

[a] Clinical information is missing from some patients in the TME cohort.

[b] In the TMA cohort, there are 211 lung adenocarcinoma patients used in the survival analysis. Out of the 211 patients, there are 52 patients with SUV_{max} data that were included in the GFAT2-SUV_{max} correlation validation.

[c] Age information is not available.

Abbreviations: RG, Radiogenomics cohort; TME, Tumor Microenvironment cohort; TCGA, The Cancer Genome Atlas; TMA, Tissue Microarray Cohort